

1
2
3
4
5
6
7
8
9
10
11
12
13
14
15
16
17
18
19
20
21
22
23
24
25
26
27
28
29
30
31

Anomalous blocking over Greenland preceded the 2013 extreme early melt of local sea ice

Thomas J. Ballinger^{1,*}, Edward Hanna², Richard J. Hall², Thomas E. Cropper³, Jeffrey Miller^{4,5},
Mads H. Ribergaard⁶, James E. Overland⁷, and Jacob L. Høyer⁶

¹Department of Geography, Texas State University, San Marcos, TX, USA

²School of Geography, University of Lincoln, Lincoln, UK

³School of Earth and Ocean Sciences, Cardiff University, Cardiff, UK

⁴Cryospheric Sciences Laboratory, NASA Goddard Space Flight Center, Greenbelt, MD, USA

⁵KBRWyle, Inc, Houston, TX, USA

⁶Danish Meteorological Institute, Copenhagen, DK

⁷NOAA/Pacific Marine Environmental Laboratory, Seattle, WA, USA

Manuscript submitted for 'Polar Ice, Polar Climate, Polar Change' special issue of
Annals of Glaciology on 20 June 2017

Revision submitted on 11 September 2017

*Corresponding Author's Address: 601 University Drive, San Marcos, Texas 78666, USA

Email: tballinger@txstate.edu

32 **ABSTRACT**

33 The Arctic marine environment is undergoing a transition from thick multi-year to first-
34 year sea ice cover with coincident lengthening of the melt season. Such changes are
35 evident in the Baffin Bay-Davis Strait-Labrador Sea (BDL) region where melt onset has
36 occurred ~ 8 days decade⁻¹ earlier from 1979-2015. A series of anomalously early events
37 has occurred since the mid-1990s, overlapping a period of increased upper-air ridging
38 across Greenland and the northwestern North Atlantic. We investigate an extreme early
39 melt event observed in spring 2013
40 ($\sim 6\sigma$ below the 1981-2010 melt climatology), with respect to preceding sub-seasonal mid-
41 tropospheric circulation conditions as described by a daily Greenland Blocking Index (GBI).
42 The 40-days prior to the 2013 BDL melt onset are characterized by a persistent, strong 500
43 hPa anticyclone over the region (GBI $> +1$ on $> 75\%$ of days). This circulation pattern
44 advected warm air from northeastern Canada and the northwestern Atlantic poleward
45 onto the thin, first-year sea ice and caused melt about 50 days earlier than normal. The
46 episodic increase in the ridging atmospheric pattern near western Greenland as in 2013,
47 exemplified by large positive GBI values, is an important recent process impacting the
48 atmospheric circulation over a North Atlantic cryosphere undergoing accelerated regional
49 climate change.

50 **KEYWORDS:** Greenland, blocking, GBI, sea ice, melt onset, sea surface temperature

51

52 **INTRODUCTION**

53 One notable product of Arctic amplification, the enhanced warming of high northern
54 latitude air temperatures relative to the Northern Hemisphere mean, is a change in the
55 seasonality of sea ice melt toward increasing periods of open water (Overland and others,
56 2016; Tonboe and others, 2016). The waters along west Greenland represent one Arctic
57 region characterized by progressively longer melt duration (Stroeve and others, 2014).
58 Extension of the open water season has been accompanied by late spring/early summer
59 decreases in albedo and increases in shortwave absorption into melt ponds and the open
60 ocean along the marginal ice zone, accelerating the sea ice-albedo feedback (Curry and
61 others, 1995; Stroeve and others, 2014). Cloud cover and water vapor feedbacks
62 influenced by sea ice losses and moisture flux into the Arctic also induce air temperature
63 warming and prolong melt conditions (Serreze and Barry, 2011).

64 In addition to recent summertime sea surface warming trends in Baffin Bay (Myers
65 and Ribergaard 2013; Comiso and Hall 2014), simultaneous, physically-related mid-
66 tropospheric geopotential height (GPH) increases that promote upper-air anticyclonic
67 ridging features have been noted across the region through development and analyses of
68 the Greenland Blocking Index (GBI; Hanna and others, 2016). Greenland blocks impact
69 local cryosphere melt (e.g. Hanna and others, 2014; Stroeve and others, 2017), and are also
70 linked to weather and climate patterns in the middle latitudes (Overland and others, 2012
71 and 2015; Hanna and others, 2016; Chen and Luo, 2017; Budikova and others, 2017) and
72 other parts of the Arctic (Ballinger and others, 2014). Recent work by Ballinger and others
73 (2017) identified an increase in the intensity and occurrence of autumn blocking over

74 Greenland (September–December) that has contributed to the region’s maritime warming
75 and the increase of open water duration west of the island.

76 While GBI conditions play a dynamical role in extending the local melt season, less is
77 known about the influence of upper-air anticyclones on changes in the timing of spring
78 melt. Trend analyses of passive microwave-derived marginal sea-ice melt and freeze dates
79 by Stroeve and others (2014) revealed a statistically significant (99% level) change toward
80 earlier melt in Baffin Bay from 1979-2013. The spring 2013 melt onset (MO) observed
81 across Baffin and waters extending southward into Davis Strait and Labrador Sea
82 (hereafter termed BDL) is particularly striking. The 2013 MO occurred on 12 April, nearly
83 2 months earlier than the 1981-2010 climatological melt of the region (9 June) and several
84 weeks before the next earliest melt occurrence (1995) in the record. This unusually early
85 melt event followed exceptionally high surface air temperature anomalies of +7.7-8.6°C
86 along the west coast of Greenland in March 2013 (Tedesco and others, 2013).

87 Given the rapidly changing seasonality of the BDL ice cover, and lack of knowledge
88 regarding the physical causes of melt anomalies in 2013 and other recent years, we utilize a
89 new, daily GBI dataset to provide an initial framework to better understand the precursor
90 role of local atmospheric circulation on early melt events. We place emphasis on the
91 preceding, sub-seasonal dynamic and thermodynamic controls of MO, as atmosphere-ocean
92 interactions within this timeframe (i.e. out to ~90-days) have been shown to dramatically
93 impact springtime sea ice melt signatures across the Arctic (e.g. Drobot and Anderson,
94 2001b; Mortin and others, 2016). GBI and early BDL MO linkages are supplemented with a
95 number of ocean-atmosphere composite analyses to further compare precursor conditions
96 of extreme melt events and evaluate the causes of the large 2013 anomaly.

97 **DATA AND METHODS**

98 Daily 25 km gridded passive microwave brightness temperatures obtained from the
99 Scanning Multichannel Microwave Radiometer and Special Sensor Microwave/Imager
100 products are used to calculate MO, which is identified as the day of year when skin
101 temperatures $>0^{\circ}\text{C}$ persist over a marine area and either surface water on snow or open
102 ocean is observed (Markus and others, 2009). This MO dataset spans Baffin Bay, Davis
103 Strait, and Labrador Sea (**Fig. 1**) and covers the period of 1979-2015. MO is primarily
104 determined from three quantities: daily difference in the 37 GHz vertically polarized
105 brightness temperatures (v_{37}), daily difference in the gradient of the 37 GHz and 19 GHz
106 vertically polarized brightness temperatures (v_{19}) adjusted for sea ice concentration, and
107 daily difference in the quantity $P = v_{19} + 0.8 v_{37}$ (Smith, 1998). The three quantities are
108 normalized, given a low-pass filter to remove noise, and summed. The top five values of
109 that sum are compared with the results from the 3x3 pixel box centered on the pixel under
110 consideration, and the MO date is determined based on the highest spatial agreement (e.g.
111 if one result matches four of the surrounding pixels and the next matches only two, the first
112 result is selected as MO).

113 The algorithm, described in Markus and others (2009), uses NASA Team ice
114 concentration (IC; Cavalieri, 1996) to validate the MO result. Primarily in the marginal ice
115 zones, MO is coincident with the disintegration of the sea ice. The algorithm checks for sea
116 ice in the middle of the year, and if the IC is 0%, the algorithm searches back in time for the
117 last day where the IC was above 80%. This IC result is compared with the algorithm result
118 from the previous section prior result and the earliest day of the two represents MO.

119 GBI daily data are calculated based on NCEP/NCAR reanalysis (Kalnay and others,
120 1996) 500 hPa GPH data downloaded for a grid of 35 well-distributed points that are then
121 averaged to produce daily GBI values, and normalized to the 1951-2000 period for the
122 standard GBI region of 60-80°N, 20-80°W. Daily data are an extension of monthly GBI time
123 series presented in Hanna et al. (2016). For consistency in supplemental atmospheric
124 analyses, we utilize NCEP/NCAR data fields to create a number of composites involving
125 GPH, sea-level pressure (SLP), meridional wind, air temperature, turbulent sensible and
126 latent heat fluxes, precipitable water, and omega (vertical atmospheric motion).

127 Additional climate modes previously associated with North Atlantic climate and
128 cryosphere variability (e.g. Lewis and others, 2017) are selected to supplement the GBI and
129 related composite analyses, including the North Atlantic Oscillation (NAO) and Atlantic
130 Multidecadal Oscillation (AMO). The daily NAO index version utilized here is the station-
131 based product of Cropper and others (2015), which represents the normalized (1951-
132 2000) SLP difference between Iceland and the Azores. The AMO index represents the
133 unsmoothed monthly sea surface temperature (SST) with trend included, spanning 0-70°N
134 within the North Atlantic basin, based on the Kaplan and others (1998) SST dataset.

135 Regional SSTs are analyzed for Baffin Bay, north and south portions of Labrador Sea,
136 and Irminger Sea, whose waters are directed towards and supply heat to eastern Baffin Bay
137 by the East and West Greenland Current (Myers and others, 2009; Myers and Ribergaard,
138 2013). A multi-dataset product is used that incorporates satellite observations from the
139 Pathfinder Advanced Very High Resolution Radiometer Version 5.2 (Casey and others,
140 2010) and the Along-Track Scanning Radiometer Reprocessing for Climate datasets
141 (Embury and others, 2012), and in-situ observations from the International

142 Comprehensive Ocean-Atmosphere Dataset Version 2.5 (Woodruff and others, 2011). An
143 interpolation method described by Høyer and others (2014) is applied to create the SST
144 product, which consists of daily, gap-free fields from 1982-2012 at a 0.05° horizontal
145 resolution. Using the same grid, the SST record has been extended to 2015 with an
146 operational product based on near real-time satellite observations, which have been
147 compared to and show agreement with the multi-dataset product previously described.
148 Arctic SST data from the Met Office Hadley Centre sea ice and SST dataset (HadISST1;
149 Rayner and others, 2003) are used to supplement the regional SST and AMO datasets.

150 To gain an idea of the optimal, pre-melt time periods when the regional, mid-
151 tropospheric circulation described by the GBI may strongly precondition sea ice for
152 continuous melt, we initially examine lagged correlations between composite, daily GBI
153 values and observed MO dates. Given a focus on sub-seasonal linkages, average GBI values
154 are initially examined over consecutive 10, 15, and 30-day periods out to 90-days prior to
155 melt in an attempt to identify robust temporal associations (latter two periods not shown).
156 The 10-day GBI aggregations exhibit the most robust covariance with the sea ice, especially
157 in the 40-days prior to melt, and are selected for subsequent analyses. Separate series of
158 lagged Pearson correlations are conducted, one with undetrended values to assess the role
159 of climatic changes in the GBI-MO relationship and another with the datasets linearly
160 detrended (DT) to evaluate interannual fluctuations, including covariations of extremes, in
161 the datasets. A two-tailed t-test (e.g. Wilks, 2011) is applied to address significance in the
162 results given a threshold of $p \leq 0.05$. Resulting lagged associations are utilized to constrain
163 the temporal limits of the composite analyses preceding melt events with particular
164 emphasis placed on 2013.

165 Prior to analyses involving the passive microwave (PM) MO data from Markus and
166 others (2009), further quality-control measures are initially undertaken. To determine if
167 the 2013 anomalous early MO was “real” and not due to instrumental errors, we surveyed
168 the daily brightness temperature maps for data artifacts, and did not find evidence of
169 sensor-related errors. As a next step, we compared the PM MO dates with those derived by
170 the Advanced Horizontal Range Algorithm (AHRA; Drobot and Anderson 2001a). AHRA
171 time series for the BDL region (Bliss and Anderson 2014) exhibit a similar dip in 2013 as
172 the PM time series with MO occurring on 1 April, which is $\sim 3\sigma$ below the 1981-2010 mean
173 MO date (1 May; A. Bliss, pers. comm.), thus showing this particular year’s extreme melt to
174 be robust to the method selected.

175 **RESULTS**

176 **Climatological Assessment of 2013 Melt Onset**

177 PM imagery portraying long-term MO and the 2013 event in the BDL region and
178 surrounding areas are shown in **Figure 2**. While much of Baffin Bay shows intermixed
179 pixels of ± 10 day deviations from normal in 2013, there is a rather notable northeast to
180 southwest trending swath of early melt anomalies (~ -40 days) that extends along the ice
181 edge from $\sim 75^\circ\text{N}$ in northeastern Baffin Bay to roughly 60°N around the southern tip of
182 Baffin Island (**Fig. 2c**). The 2013 early melt event (day of year 102; 12 April) is particularly
183 anomalous relative to MO dates archived across the modern satellite record (**Fig. 3**) at
184 almost six standard deviations (6σ) below the 1981-2010 mean BDL MO date, and is
185 roughly 8 weeks earlier than normal MO (day of year 160; 9 June). It is apparent from
186 **Figure 3** that progressively earlier melt conditions are a clear feature of the recent BDL

187 spring environment, though the 2013 region-wide melt is an outlier, beginning 38 days
188 earlier than the next earliest melt observed in 1995 (day of year 140; 20 May).

189 **Atmospheric Circulation Anomalies**

190 Based on the lagged correlations, especially involving the detrended time series, the
191 optimal GBI linkage with subsequent MO is found within the 40-day period preceding melt
192 ($r_{DT} < -0.35$, $p \leq 0.05$ in all 10-day windows out to 40 days; **Table 1**). Visual inspection of the
193 detrended time series (**Supplemental Fig. 1**) reveals pronounced anti-correlation during
194 the earliest melt years where positive GBI occurrences are anomalously high pre-dating
195 MO.

196 To initially assess the physical contributions to anomalous sea ice melt events, the
197 synoptic atmospheric circulation is evaluated through analyses of the GBI over the 40-day
198 timeframe preceding extreme MOs (characterized as 1σ events below the climatological
199 BDL melt date). Early melt years are typically defined by positive, daily GBI conditions
200 during at least half of the days in this timeframe, with many of these occurring within the
201 10 to 15-day period immediately prior to melt (**Fig. 4**). The 2013 event is characterized by
202 positive GBI values persisting throughout the 40-days leading up to melt ($\mu_{GBI} = 1.46$) with
203 31 days exhibiting GBI values of at least +1, of which 10-days observed index values $> +2$
204 (**Table 2**). The preponderance of +1 and +2 extreme daily GBI values represent a
205 statistically significant increase from climatology by roughly a factor of 4 and 5,
206 respectively. Similar to 2013, the 2010 pre-melt period exhibits 40 consecutive days of
207 positive GBI values, while the 1995 melt coincides with 9 days of GBI values $\geq +2$. The latest
208 melt onsets of the 1980s and early 1990s, by contrast, are characterized by greater GBI
209 variability with fewer positive GBI days and more frequent negative extreme occurrences

210 (Supplemental Table 1 and Supplemental Fig. 2), reflecting the colder ocean-
211 atmosphere state of the region relative to the years that followed (Buch and others, 2004;
212 van As, 2011). These case studies identify the unparalleled nature of the 2013 event in
213 terms of extreme GBI persistence before MO with values remaining $\geq +1$ for 26 consecutive
214 days (day 40 to day 14; Fig. 4), and 500 hPa GPH anomalies of +300 m over Baffin Bay
215 during the 21-to-30 days before melt (not shown).

216 Composite 500 hPa GPH analyses reveal notable circulation differences between the
217 set of early melt years (Fig. 5). In particular, strong high pressure blocking is shown across
218 the BDL region in 2013, with mean height anomalies of $\geq +160$ m spanning much of the area
219 and extending into the Central Arctic Ocean. Mid-tropospheric GPH anomalies are similarly
220 above-normal in the next earliest years of 1995 and 2010 across the North Atlantic and
221 Greenland, but exhibit lower heights over the BDL area by 40-80 m during their respective
222 pre-melt periods relative to the 2013 event. Positive (anticyclonic) 500 hPa GPH anomalies
223 favor meridional flow as indicated by prevailing southerly winds observed blowing south-
224 to-north across Davis Strait (60-65°N, 52.5-62.5°W) from the polar front jet level (300 hPa)
225 to the lower troposphere (925 hPa; not shown). These anomalous flows are not evident for
226 1998, 2003 and 2012, which have MO anomalies closer to 1σ below normal.

227 Poleward advection of lower-latitude air onto the BDL ice cover in 2013 is also
228 impacted by a weaker-than-normal North Atlantic surface pressure gradient. Average
229 values of the Cropper NAO index over the 40-day window are 2.16σ below the
230 climatological mean, which is substantially more negative than the next lowest NAO value
231 observed during an extreme melt year (-0.93 in 1995). In 2013, the Icelandic Low shows
232 significant weakening from normal with positive sea-level pressure values of $\sim +16$ -20 hPa

233 extending from northern Irminger Sea northward onto the eastern half of the island and
234 adjacent Greenland Sea. Positive SLP anomalies of +8-12 hPa also extend into the BDL
235 area, while a significantly weakened Azores High with below-normal pressure is found
236 across the northeastern Atlantic (**Supplemental Fig. 3**). Persistent positive surface
237 pressure and mid-tropospheric height anomalies over the BDL region favor southerly,
238 geostrophic airflow from the comparatively warmer environment of the western North
239 Atlantic through Davis Strait and into Baffin Bay, thereby preconditioning the seasonal sea
240 ice for abnormally early melt.

241 **Thermodynamic Environment**

242 Collocated with the persistent and strong, upper-level high pressure Greenland
243 block in 2013 are positive T850 anomalies of $>+6^{\circ}\text{C}$ oriented in a south-to-north manner
244 along Davis Strait that extend into Baffin Bay (**Fig. 6**). Aside from 1998 and 2012, the
245 remaining early melt years are led by positive temperature anomalies over waters adjacent
246 to the west Greenland coastline, though none are comparable to the magnitude of warm
247 anomalies in 2013.

248 To further investigate the nature of the 2013 warm air temperatures over the BDL
249 during the unusually strong and persistent Greenland Block, we initially examine the
250 regional SST conditions. Over the 40-days preceding melt, SST anomalies are slightly
251 positive in Baffin Bay (**Table 3**), narrowly above the salinity-adjusted freezing point in an
252 area often characterized by sub-freezing temperatures and seasonal sea ice coverage
253 during this time (not shown). Northern and southern portions of the Labrador Sea also
254 exhibit positive SST anomalies of $+0.13^{\circ}\text{C}$ and $+0.47^{\circ}\text{C}$, respectively, while the surface
255 waters within Irminger Sea are $+0.37^{\circ}\text{C}$ from the 1982-2011 average. The precursor North

256 Atlantic-wide ocean temperature departures categorized by the March 2013 AMO index
257 value are anomalous (+0.17°C), falling within the uppermost quartile of SST values
258 beginning in 1982. In addition, HadISST1 also shows a swath of +0.50-1.50°C SST
259 anomalies extending south from the southwest Greenland coast, representing a source of
260 lower latitude warm air swept north across the ice by prevailing winds (**Supplemental Fig.**
261 **4**).

262 Positive air temperature anomalies extend from the surface to the middle
263 troposphere over the BDL region (**Fig. 7**) with the largest departures ($\sim+8^{\circ}\text{C}$) near the
264 surface, emanating southward from southern Baffin Bay ($\sim 69^{\circ}\text{N}$) into northern Labrador
265 Sea ($\sim 63^{\circ}\text{N}$). Conductive heat flux from the relatively warm ocean surface to the adjacent
266 cooler atmosphere may slightly influence the anomalously warm lower tropospheric air
267 temperature anomalies, however persistent high pressure and on-ice flow likely has a
268 greater impact on melt. Small, negative latent and sensible heat flux anomalies over areas
269 of seasonal ice coverage (**Fig. 8a,b**) suggest transfers of atmospheric moisture and heat
270 toward the surface. Descending motion, while pronounced over southern Greenland, is
271 also relatively weak in BDL areas as indicated by positive 500 hPa omega anomalies (**Fig.**
272 **8c**). Poleward-flowing thermal winds, corroborated by the meridional wind anomaly
273 extending westward from central Davis Strait, are associated with large, positive 1000-500
274 hPa thickness anomalies that reinforce the concurrent blocking regime in transporting a
275 warm, moist layer of air over the Labrador Sea northward onto the BDL ice cover before
276 melt ensues (**Fig. 8d,e,f**).

277 **DISCUSSION**

278 A confluence of precursor dynamical and thermodynamic conditions influenced the
279 unseasonably early melt of the 2013 BDL ice cover. Foremost, positive 500 hPa height
280 anomalies, assessed from the GBI time series and shown via composite analyses, persisted
281 in the immediate 40-day window before melt. Stationary, upper-air ridges are not
282 uncommon in this region in the weeks-to-months preceding the spring break-up; however,
283 the magnitude of the persistent 500 hPa GPH pattern observed in 2013 is unprecedented
284 preceding MO events during the PM satellite record. Downstream linkages to the GBI
285 anomaly also manifested in a record low Hurrell PC-based March NAO index value back to
286 1899 (Hanna and others, 2015) and the coldest UK-wide March temperatures since 1962
287 (Met Office 2013).

288 Since the early 1990s, GBI values have increased during the cold season when
289 seasonal ice cover forms and persists in the BDL region (November-March; Hanna and
290 others, 2016). Amplified upper-level heights in winter (DJF) and spring (MAM) across
291 Greenland tend to coincide with a weak North Atlantic polar front jet stream and enhanced
292 meridional circulation of warm air from the Irminger and Labrador Seas and northeastern
293 Canada into Baffin Bay (Hanna and others, 2016). The synoptic ocean-atmosphere
294 conditions associated with the 2013 BDL melt anomaly are characterized by anomalous
295 blocking, meridional flow and relatively mild air temperatures with slightly above-average
296 Labrador and Irminger SSTs that directly interact with the ice cover through regional
297 hydrography involving the East Greenland Current. Local SSTs in sea-ice free areas of the
298 Arctic influence low-to-middle troposphere warming through ocean-atmosphere heat
299 exchange (Screen and others, 2012). However, the coupling of persistent and positive GBI
300 conditions and local SST anomalies does not appear to be a preconditioning requirement to

301 generate an anomalously early BDL MO. For example, the 40-day period preceding both
302 the 2010 and 2013 early melt events are categorized by positive local SST conditions and
303 GBI values, while the pre-melt period during the 1995 event witnessed above-average GBI
304 conditions amidst negative SST anomalies (not shown). Comparatively, the 2010 SST
305 anomalies in N/S Labrador Sea and Baffin Bay were the warmest or second warmest pre-
306 dating MO, while those regions only saw slight ocean temperature deviations from
307 climatology in 2013. These findings, along with the turbulent flux and omega anomalies
308 shown in **Fig. 8**, suggest that air temperature anomalies extending from the surface to
309 ~400 hPa were influenced slightly by downward shortwave flux and SSTs with a larger
310 warming contribution from warm air advection due to the presence of persistent high
311 pressure about the region.

312 The 2013 anomalous climatic event marked the second notable period of GBI
313 persistence that dramatically impacted the North Atlantic cryosphere within the space of a
314 year. Summer (JJA) 2012 also witnessed record-breaking GBI values (over the NCEP/NCAR
315 record from 1948 onward) and the Greenland Ice Sheet experienced historic spatial melt
316 extent (Nghiem and others, 2012; Hanna and others, 2014). Above-average coastal air and
317 ocean surface temperatures persisted into autumn 2012 bringing about the second latest
318 Baffin freeze onset in the PM record (Ballinger and others, 2017). The duration of the
319 freeze period, from 17 November 2012 to 12 April 2013 and nearly 2.5 months shorter-
320 than-normal, is the shortest such window of the PM record (**Supplemental Fig. 5**).
321 Correlation analyses indicate that freeze duration and MO strongly co-vary through time
322 ($r=+0.90$, $r_{DT}=+0.87$, $p<0.05$ in both cases) with anomalously early melt generally
323 connected to abbreviated periods of freezing temperatures. Delays in autumn freeze onset

324 also appear to influence this relationship by promoting earlier melt the following spring
325 ($r=-0.50$, $p<0.05$). It is likely that the short period of ice coverage in 2013 also coincided
326 with a thinner-than-normal seasonal ice pack as December 2012-March 2013 near-surface
327 air temperature anomalies (from NCEP/NCAR reanalysis) were $\sim+5^{\circ}\text{C}$ above-normal
328 across Baffin Bay (Peings and Magnusdottir, 2015).

329 **CONCLUSIONS**

330 The Arctic amplification signal has emerged from climate system noise over the last
331 two decades, creating complex, bidirectional linkages between meridional airflow and the
332 background thermodynamic state based on behaviors of variables such as sea ice and SSTs
333 that vary by regional geography (Francis and Vavrus, 2015; Overland and others, 2016). In
334 this study, persistence of a strong Greenland blocking anticyclone across a 40-day period in
335 late winter/early spring of 2013 prompted an unusually early and continuous melt of
336 seasonal ice cover across Baffin Bay, Davis Strait, and the Labrador Sea. The stationary
337 high pressure pattern was the primary mechanism responsible for relatively warm
338 temperatures in the lower-to-middle-troposphere, driving localized heating through the
339 transport of warm, moist air onto the thin ice cover. We posit that an abnormally short
340 freeze period also played a role in preconditioning the ice cover for extreme melt. Future
341 studies will further examine freeze duration links to melt onset in a regional sea ice-
342 atmosphere context.

343 In addition to temperature advection, poleward moisture flux has been linked with
344 Arctic warming through increases in cloud coverage and downward infrared radiation
345 (Gong and others, 2017). Early sea ice melt events across the Arctic often coincide with a
346 steady increase in atmospheric water vapor over the two-week period leading up to melt,

347 followed by a rapid drying of the atmosphere thereafter (Mortin and others, 2016). In this
348 study, persistent, high pressure anomalies extending up to the 500 hPa layer likely
349 influenced poleward temperature and moisture advection, but precluded extremely high
350 local humidity values from occurring, though detailed analyses of water vapor content
351 were not explicitly conducted for 2013 or other early melt events. As the transport of heat
352 and moisture fluxes into the Arctic are strongly influenced by variations in the polar jet
353 stream, it is imperative to continue to conduct analyses with regional circulation modes
354 such as the GBI to advance understanding of the precursor dynamical forcing associated
355 with snow, glacier, and sea ice melt anomalies.

356 **ACKNOWLEDGEMENTS**

357 Angela Bliss, Ronald Kwok, and Thomas Mote are thanked for discussions of local
358 glaciology during spring of 2013. We appreciate comments from Walt Meier (editor) and
359 two anonymous reviewers, which helped to improve the manuscript.

360 The National Oceanic and Atmospheric Administration (NOAA) Earth System Research
361 Laboratory (ESRL) Physical Sciences Division (PSD) website provided NCEP/NCAR
362 reanalysis data (<https://www.esrl.noaa.gov/psd/data/gridded/data.ncep.reanalysis.html>)
363 AMO monthly time series (<https://www.esrl.noaa.gov/psd/data/timeseries/AMO/>), and
364 the Web-based Reanalysis Intercomparison Tool used to create the HadISST March 2013
365 SST anomaly plot (<https://www.esrl.noaa.gov/psd/cgi-bin/data/testdap/plot.comp.pl>).

366 Data are available upon request. JEO is supported by Arctic Research of NOAA's Climate
367 Program Office. This is PMEL contribution number 4679.

368

369 **REFERENCES**

370

371 Ballinger TJ, Sheridan SC and Hanna E (2014) Resolving the Beaufort Sea High using
372 synoptic climatological methods. *Int. J. Climatol.*, **34**, 3312-3319
373 (doi:10.1002/joc.3907)

374

375 Ballinger TJ, Hanna E, Hall RJ, Miller J, Ribergaard MH and Høyer JL (2017) Greenland
376 coastal air temperatures linked to Baffin Bay and Greenland Sea ice conditions during
377 autumn through regional blocking patterns. *Clim. Dyn.*, in press (doi:10.1007/s00382-
378 017-3583-3)

379

380 Bliss AC and Anderson MR (2014) Arctic sea ice melt onset from passive microwave
381 satellite data: 1979-2012, *The Cryosphere*, **8**, 2089–2100 (doi:10.5194/tcd-8-2089-
382 2014)

383

384 Buch E, Pedersen SA and Ribergaard MH (2004) Ecosystem variability in West Greenland
385 waters. *J. Northwest Alt Fish Sci*, **34**, 13-28 (doi:10.2960/J.v34.m479)

386

387 Budikova D, Ford TW and Ballinger TJ (2017) Connections between north-central United
388 States summer hydroclimatology and Arctic sea ice variability. *Int. J. Climatol.*, in press
389 (doi:10.1002/joc.5097)

390

391 Casey KS, Brandon TB, Cornillon P and Evans R (2010) The past, present, and future of the
392 AVHRR Pathfinder SST program. *In Oceanography from space* (pp. 273-287). Springer,
393 Netherlands.

394

395 Cavalieri DJ (1996) NASA team sea ice algorithm.
396 (<http://nsidc.org/data/docs/daac/nasateam/index.html>)

397

398 Chen X and Luo D (2017) Arctic sea ice decline and continental cold anomalies: Upstream
399 and downstream effects of Greenland blocking. *Geophys. Res. Lett.*, **44**, 3411-3419
400 (doi:10.1002/2016GL072387)

401

402 Comiso JC and Hall DK (2014) Climate trends in the Arctic as observed from space. *Wiley*
403 *Int. Rev.: Clim. Change*, **5**, 389-409

404

405 Cropper T, Hanna E, Valente MA and Jónsson T (2015) A daily Azores-Iceland North
406 Atlantic Oscillation index back to 1850. *Geosci. Data J.*, **2**, 12-24 (doi:10.1002/gdj3.23)

407

408 Curry JA, Schramm JL and Ebert EE (1995) Sea ice-albedo climate feedback mechanism. *J*
409 *Climate*, **8**, 240-247

410

411 Drobot SD and Anderson MR (2001a) An improved method for determining snowmelt
412 onset dates over Arctic sea ice using Scanning Multichannel Microwave Radiometer
413 and Special Sensor Microwave/Imager data. *J. Geophys. Res. Atmos.*, **106**, 24033–24049

414

415 Drobot SD and Anderson MR (2001b) Comparison of interannual snowmelt-onset dates
416 with atmospheric conditions. *Ann. Glaciol.*, **33**, 79-84
417

418 Embury O, Merchant CJ, and Corlett GK (2012) A reprocessing for climate of sea surface
419 temperature from the along-track scanning radiometers: Initial validation, accounting
420 for skin and diurnal variability effects. *Remote Sens. Environ.*, **116**, 62-78.
421

422 Francis JA and Vavrus SJ (2015) Evidence for a wavier jet stream in response to rapid
423 Arctic warming. *Environ. Res. Lett.*, **10** (doi:10.1088/1748-9326/10/1/014005)
424

425 Gong T, Feldstein S and Lee S (2017) The role of downward infrared radiation in the recent
426 Arctic winter warming trend. *J. Climate*, **30**, 4937-4949 (doi:10.1175/JCLI-D-16-
427 0180.1).
428

429 Hanna E, Fettweis X, Mernild SH, Cappelen J, Ribergaard MH, Shuman CA, Steffen K, Wood L
430 and Mote T (2014) Atmospheric and oceanic climate forcing of the exceptional
431 Greenland ice sheet surface melt in summer 2012. *Int. J. Climatol.*, **34**, 1022-1037
432 (doi:10.1002/joc.3743)
433

434 Hanna E, Cropper TE, Hall RJ, Scaife AA and Allen R (2015) Recent seasonal asymmetric
435 changes in the NAO (a marked summer decline and increased winter variability) and
436 associated changes in the AO and Greenland Blocking Index. *Int. J. Climatol.*, **35**, 2540-
437 2554 (doi:10.1002/joc.4157)
438

439 Hanna E, Cropper TE, Hall RJ and Cappelen J (2016) Greenland Blocking Index 1851-2015:
440 a regional climate change signal. *Int. J. Climatol.*, **36**, 4847-4861
441 (doi:10.1002/joc.4673)
442

443 Høyer JL, Le Borgne P and Eastwood S (2014) A bias correction method for Arctic satellite
444 sea surface temperature observations. *Remote Sens. Environ.*, **146**, 201-213
445

446 Kaplan A, Cane M, Kushnir Y, Clement A, Blumenthal M and Rajagopalan B (1998) Analyses
447 of global sea surface temperature 1856–1991. *J. Geophys. Res.*, **103**, 18567–18589
448

449 Kalnay E, Kanamitsu M, Kistler R, Collins W, Deaven D, Gandin L, Iredell M, Saha S, White G,
450 Woollen J, Zhu Y, Chelliah M, Ebisuzaki W, Higgins W, Janowiak J, Mo KC, Ropelewski C,
451 Wang J, Leetmaa A, Reynolds R, Jenne R and Joseph D (1996) The NCEP/NCAR 40-year
452 reanalysis project. *Bull. Am. Meteorol. Soc.*, **77**, 437-471
453

454 Lewis G, Osterberg E, Hawley R, Whitmore B, Marshall HP and Box J (2017) Regional
455 Greenland accumulation variability from Operation IceBridge airborne accumulation
456 radar. *The Cryosphere*, **11**, 773-788 (doi:10.5194/tc-11-773-2017)
457

458 Markus T, Stroeve JC and Miller J (2009) Recent changes in Arctic sea ice melt onset,
459 freezeup, and melt season length. *J. Geophys. Res.*, **114**, C12024,
460 (doi:10.1029/2009JC005436)
461

462 Met Office (2013) March 2013,
463 (<http://www.metoffice.gov.uk/climate/uk/summaries/2013/march>), date of last
464 access 8 September 2017.
465

466 Myers PG, Donnelly C and Ribergaard MH (2009) Structure and variability of the West
467 Greenland Current in summer derived from 6 repeat standard sections. *Prog. Ocean.*,
468 **80**, 93-112 (doi:10.1016/j.pocean.2008.12.003)
469

470 Myers PG and Ribergaard MH (2013) Warming of the polar water layer in Disko Bay and
471 potential impact on Jakobshavn Isbrae. *J. Phys. Ocean.*, **43**, 2629-2640
472 (doi:10.1175/JPO-D-12-051.1)
473

474 Mortin J, Svensson G, Graverson RG, Kapsch L-L, Stroeve JC and Boisvert LN (2016) Melt
475 onset over Arctic sea ice controlled by atmospheric moisture transport. *Geophys. Res.
476 Lett.*, **43**, 6636-6642 (doi:10.1002/2016GL069330)
477

478 Nghiem SV, Hall DK, Mote TL, Tedesco M, Albert MR, Keegan K, Shuman CA, DiGirolamo NE
479 and Neumann G (2012) The extreme melt across the Greenland ice sheet in 2012.
480 *Geophys. Res. Lett.*, **39**, L20502 (doi:10.1029/2012GL053611)
481

482 Overland JE, Francis JA, Hanna E and Wang M (2012) The recent shift in early summer
483 Arctic atmospheric circulation. *Geophys Res Lett.*, **39**, L19804
484 (doi:10.1029/2012GL053268)
485

486 Overland JE, Francis JA, Hall RJ, Hanna E, Kim S-J and Vihma T (2015) The melting Arctic
487 and mid-latitude weather patterns: are they connected? *J. Climate*, **28**, 7917-7932
488 (doi:10.1175/JCLI-D-14-00822.1)
489

490 Overland JE, Dethloff K, Francis JA, Hall RJ, Hanna E, Kim S-J, Screen JA, Shepherd TG and
491 Vihma T (2016) Nonlinear response of mid-latitude weather to the changing Arctic.
492 *Nat. Clim. Change*, **6**, 992-999 (doi:10.1038/NCLIMATE3121)
493

494 Peings Y and Magnusdottir G (2015) Role of sea surface temperature, Arctic sea ice and
495 Siberian snow in forcing the atmospheric circulation in winter of 2012-2013. *Clim.
496 Dyn.*, **45**, 1181-1206 (doi:10.1007/s00382-014-2368-1)
497

498 Rayner NA, Parker DE, Horton EB, Folland CK, Alexander LV, Rowell DP, Kent EC and
499 Kaplan A (2003) Global analyses of sea surface temperature, sea ice, and night marine
500 air temperature since the late nineteenth century. *J. Geophys. Res.*, **108**, 4407
501 (doi:10.1029/2202JD002670,D14)
502

503 Screen JA, Deser C and Simmonds I (2012) Local and remote controls on observed Arctic
504 warming. *Geophys. Res. Lett.*, **39**, L10709 (doi:10.1029/2012GL051598)
505

506 Serreze MC and Barry RG (2011) Processes and impacts of Arctic amplification: A research
507 synthesis. *Glob. Planet. Change*, **77**, 85-96
508

509 Smith DM (1998) Observation of perennial Arctic sea ice melt and freeze-up using passive
510 microwave data. *J. Geophys. Res.*, **103**, 27,753–27,769 (doi:10.1029/98JC02416)
511

512 Stroeve JC, Markus T, Boisvert L, Miller J and Barrett A (2014) Changes in Arctic melt
513 season and implications for sea ice loss. *Geophys. Res. Lett.*, **41**, 1216–1225
514 (doi:10.1002/2013GL058951)
515

516 Stroeve JC, Mioduszewski, Rennermalm A, Boisvert LN, Tedesco M and Robinson D (2017)
517 Investigating the local scale influence of sea ice on Greenland surface melt. *The*
518 *Cryosphere Discuss.*, 1-36 (doi:10.5194/tc-2017-65)
519

520 Tedesco M, Box JE, Cappelen J, Fettweis X, Jensen T, Mote T, Rennermalm AK, Smith LC, van
521 de Wal RSW and Wahr J (2013) Greenland ice sheet [in Arctic Report Card 2013],
522 <http://www.arctic.noaa.gov/Report-Card>.
523

524 Tonboe RT, Eastwood S, Lavergne T, Sørensen AM, Rathmann N, Dybkjær G, Pedersen LT,
525 Høyer JL, and Kern S (2016) The EUMETSAT sea ice concentration climate data record.
526 *The Cryosphere*, **10**, 2275
527

528 van As D (2011) Warming, glacier melt and surface energy budget from weather station
529 observations in the Melville Bay region of northwest Greenland. *J. Glaciol.*, **57**, 208-220
530

531 Wilks DS (2011) *Statistical methods in atmospheric sciences*, 3rd edn. Academic Press,
532 Oxford
533

534 Woodruff SD, Worley SJ, Lubker SJ, Ji Z, Freeman JE, Berry DI, Brohan P, Kent EC, Reynolds
535 RW, Smoth SR and Wilkinson C (2011) ICOADS Release 2.5: extensions and
536 enhancements to the surface marine meteorological archive. *Int. J. Climatol.*, **31**, 951-
537 967.
538

539 **Tables**

Days Before Melt	Correlation Coefficients	
	r	r _{DT}
1-10	-0.32	-0.34
11-20	-0.28	-0.35
21-30	-0.48	-0.51
31-40	-0.53	-0.43
41-50	-0.16	-0.28
51-60	-0.24	-0.24
61-70	-0.13	-0.04
71-80	-0.05	+0.04
81-90	+0.01	-0.02
1-40	-0.62	-0.64

540

541 **Table 1.** Lagged Pearson’s correlations of GBI composite values within different time
 542 windows preceding each respective BDL melt onset (MO) versus MO day of year. Linearly
 543 detrended analyses are indicated as such (r_{DT}). Bold values are significant at p≤0.05.
 544

545

Time Period	GBI Descriptive Statistics		Σ GBI Days (n)					
	μ	σ	≤ -2	≤ -1	≤ 0	> 0	≥ 1	≥ 2
Climatology (1981-2010)	0.10	0.29	0.13	6.03	19.73	20.27	7.67	2.23
2013	1.46	0.74	-	-	-	40	31	10
1995	1.12	1.05	-	-	9	31	24	9
2010	0.92	0.44	-	-	-	40	12	2
2003	0.11	0.72	-	1	15	25	5	-
1998	0.05	0.49	-	-	20	20	2	-
2012	0.12	0.60	-	-	21	19	4	-

546

547 **Table 2.** GBI descriptive statistics (mean= μ , sigma= σ) and sum (Σ) of days at different GBI
 548 value thresholds for the 40-day period preceding MO across the climatological normal
 549 period and the early melt years. Significant differences, determined by a two-tailed t-test
 550 ($p \leq 0.05$), between GBI occurrences in the six year's presented and climatology are shown
 551 in bold (where threshold of occurrence is at least 5% of days, $n=2$).
 552

553

Domain	SST anomaly (°C)	Rank
Baffin Bay	>+0.01	5
Irminger Sea	+0.37	13
North Labrador Sea (NLS)	+0.13	13
South Labrador Sea	+0.47	11
NLS _{65°N, 57.5°W}	-0.10	9
NLS _{64°N, 57.5°W}	+0.15	9
NLS _{63°N, 57.5°W}	+0.11	12
AMO March	+0.17	4

554

555 **Table 3.** SST anomalies over the 40-day period preceding melt in 2013 (versus 1982-2011
556 climatology) and corresponding rank over the 1982-2015 period (warmest year = 1,
557 coldest year = 34). AMO March represents a monthly-averaged value. The high rank
558 despite negative anomaly at the 65°N gridpoint reflects the tendency for this North
559 Labrador Sea (NLS) location to be ice-covered with the exception of warm years. Local
560 hydrographic regions are identified in **Fig. 1**.

561

562

563

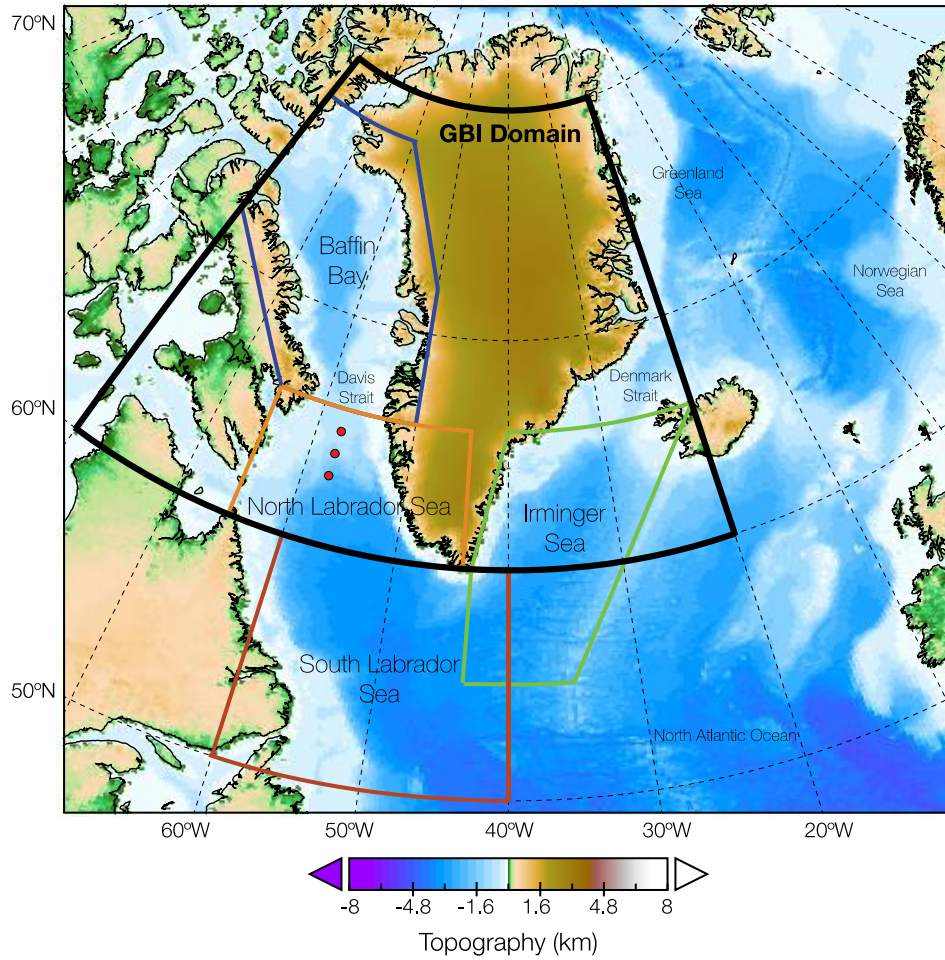
564

565

566

567

568



570
 571
 572 **Fig. 1.** Study area map identifying the GBI and regional SST domains. The red dots signify
 573 North Labrador SST gridpoints (as indicated in **Table 3**) located near the ice-ocean
 574 interface. The Baffin Bay, Davis Strait, and North/South Labrador Sea areas collectively
 575 comprise the BDL region.
 576

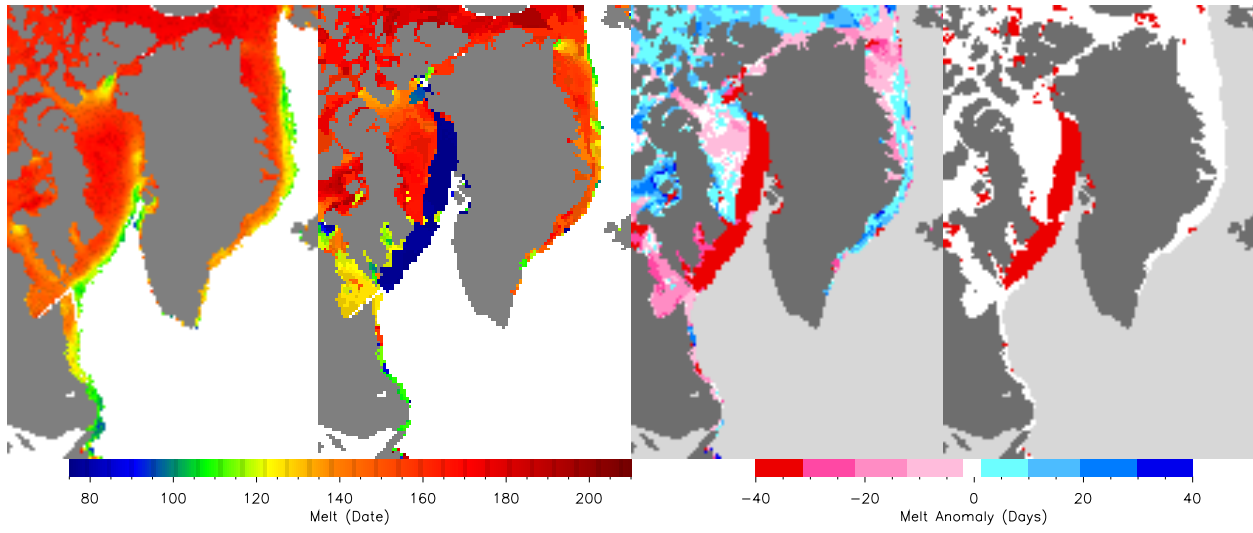
577

a) Melt Onset Climatology
1979–2015

b) 2013 Melt

c) Melt Anomaly

d) Significant Anomaly



578

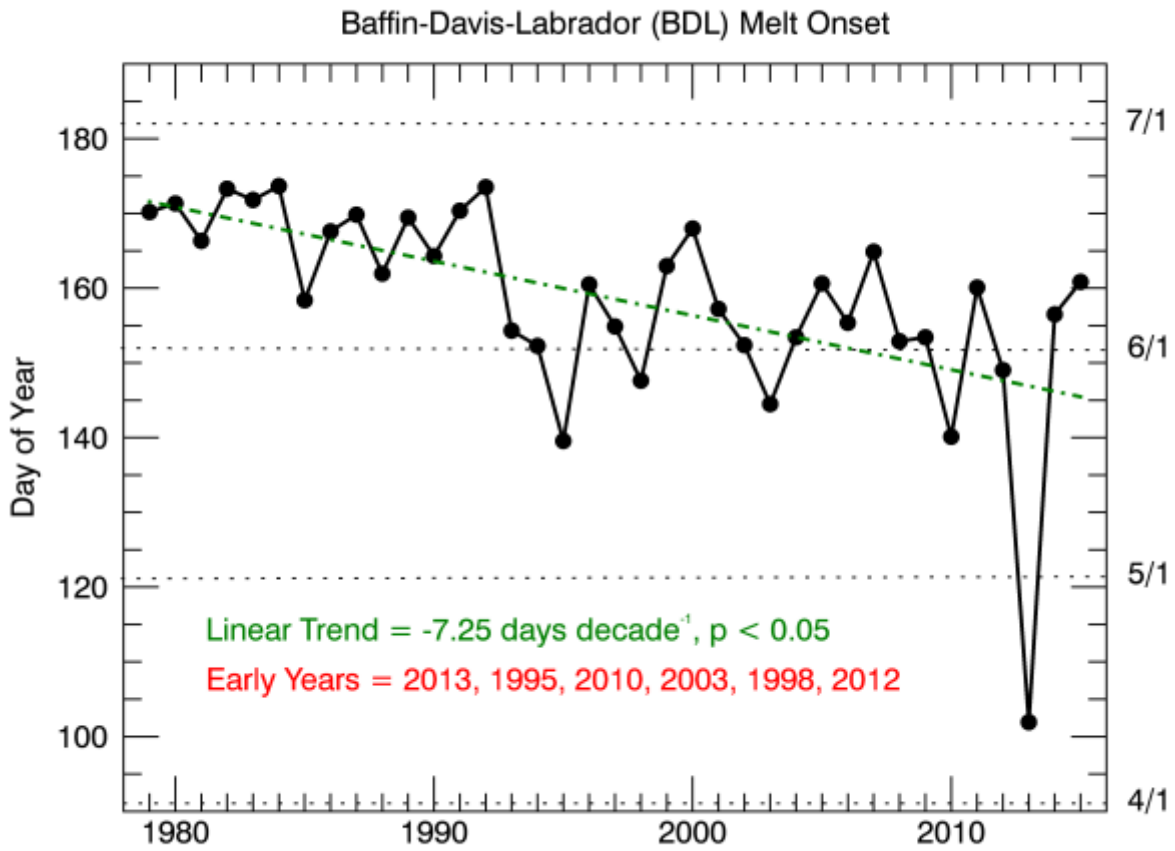
579

580 **Fig. 2.** Melt onset (MO) maps of the BDL region and surrounding areas depicting a)
581 climatological MO dates, 1979-2015, b) 2013 MO dates, c) 2013 MO anomalies (relative to
582 the 1979-2015 period), and d) areas of statistical difference from climatology (in red,
583 $p \leq 0.05$).

584

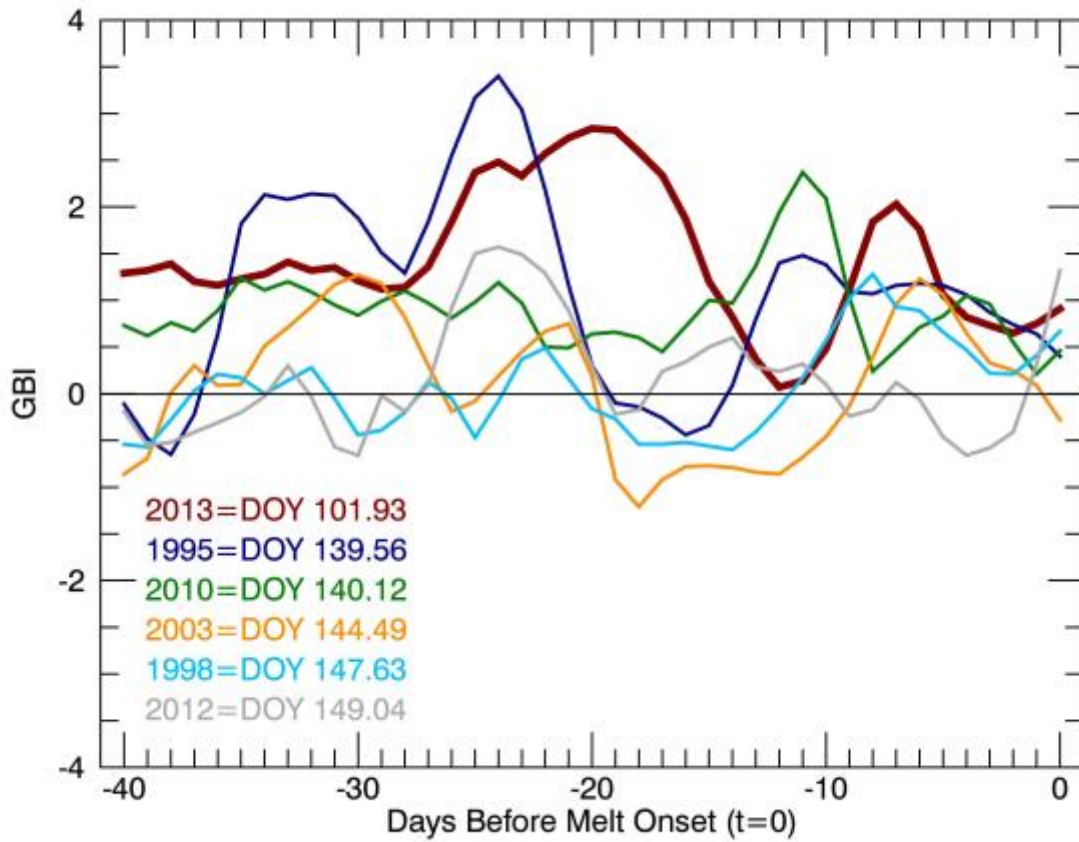
585

586



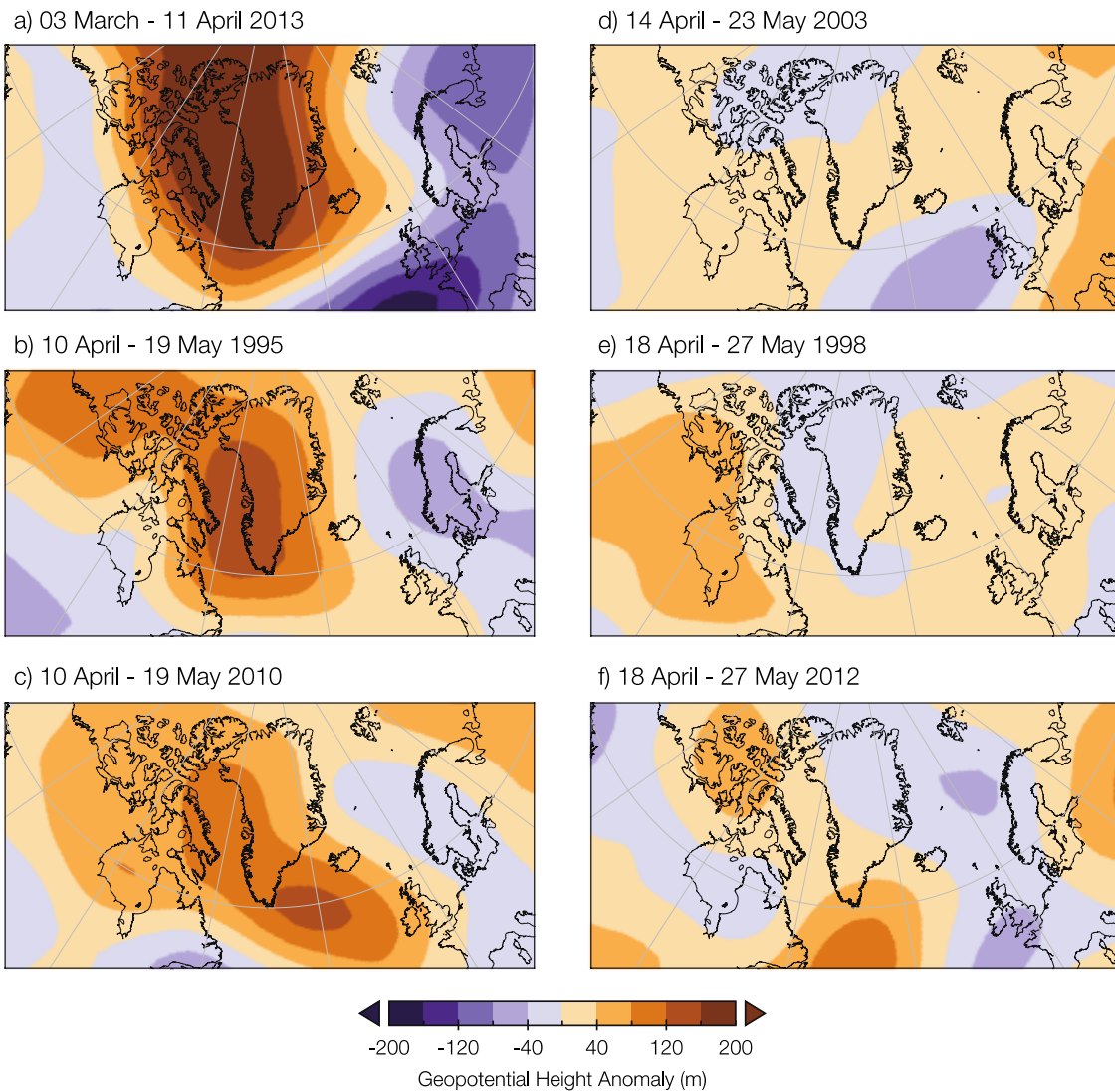
587
588
589
590
591
592
593
594

Fig. 3. Time series of BDL MO dates, 1979-2015. The left y axis represents the day of year when continuous melt occurs, while the right y axis shows the respective first day of each month (i.e. 4/1 = 1 April) in non-leap years. Early MO years, 1σ below the 1981-2010 mean, are identified within the graphic.



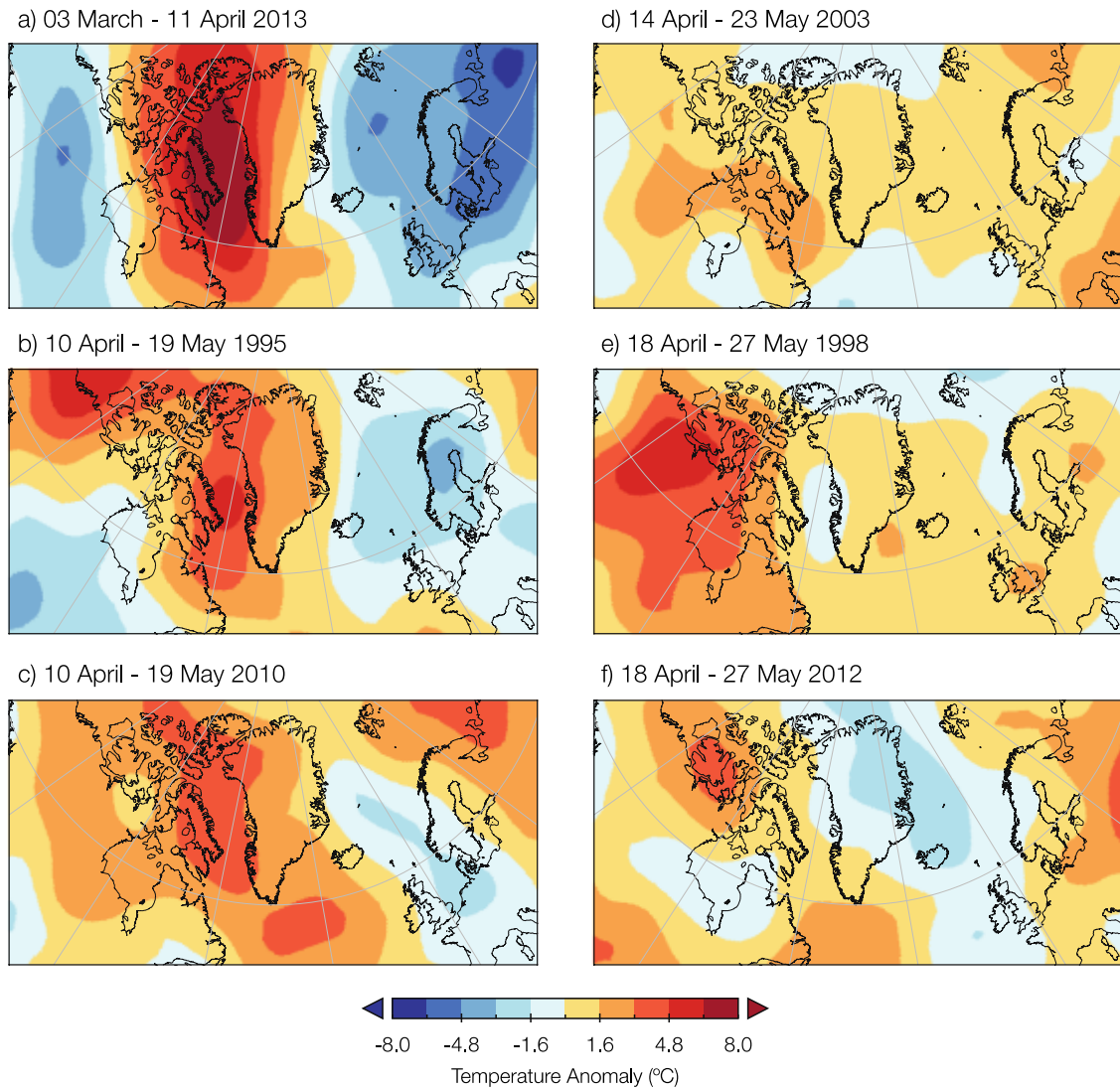
595
 596
 597
 598
 599
 600

Fig. 4. Daily GBI values during the 40-days preceding the early BDL MO years, which are listed sequentially in the bottom left of the plot with the corresponding day of year (DOY) marking continuous melt conditions for the region.



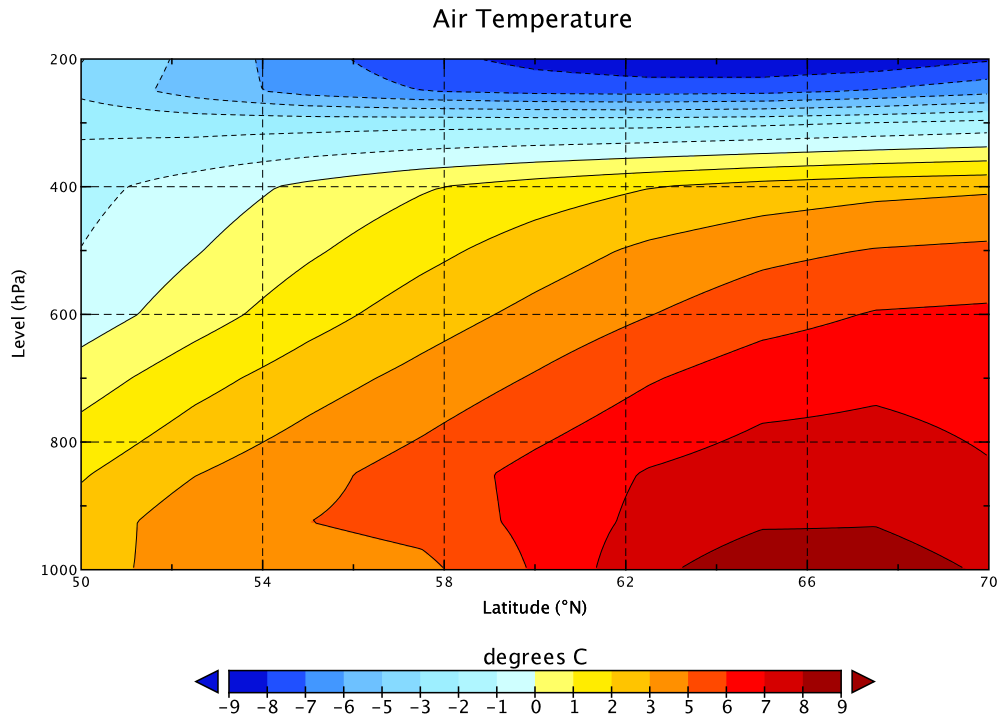
601
602
603
604
605
606
607

Fig. 5. Composite 500 hPa GPH anomaly maps, versus 1981-2010 mean, during the 40-day period referenced for a) 2013, b) 1995, c) 2010, d) 2003, e) 1998, and f) 2012 early MO years.



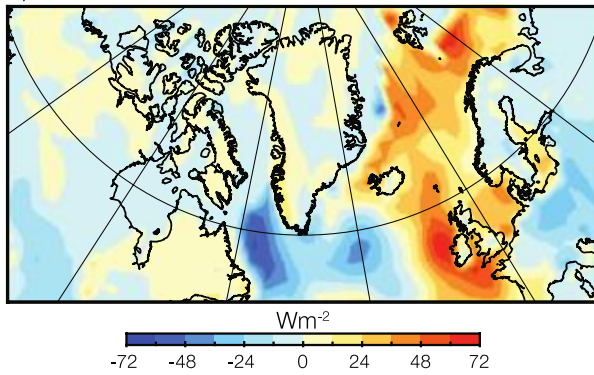
609
 610
 611
 612
 613

Fig. 6. Composite T850 hPa anomaly maps, versus 1981-2010 mean, during the 40-day period referenced for a) 2013, b) 1995, c) 2010, d) 2003, e) 1998, and f) 2012 early MO years.

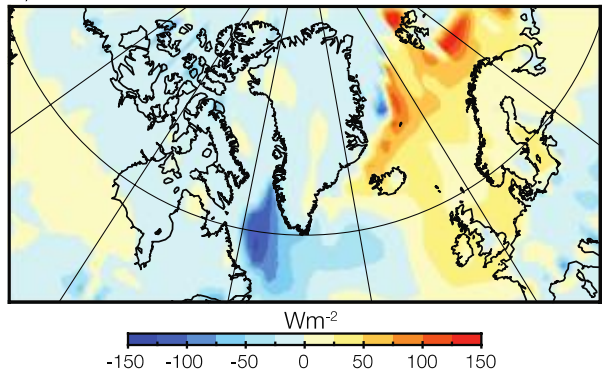


614
 615 **Fig. 7.** Vertical air temperature anomalies for 3 March – 11 April 2013 stretching from
 616 southern Baffin Bay through the Labrador Sea (50-70°N, 50-60°W) relative to the 1981-
 617 2010 mean for the 40-day period.
 618
 619

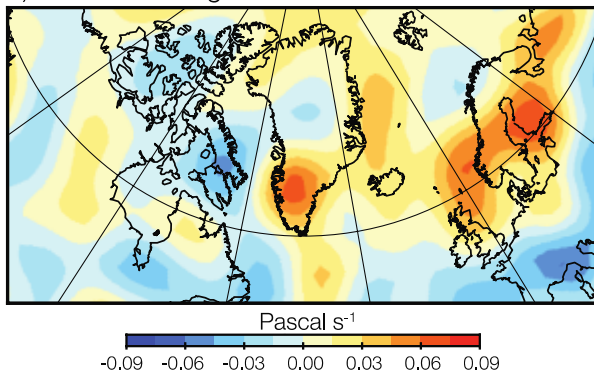
a) Latent Heat Flux



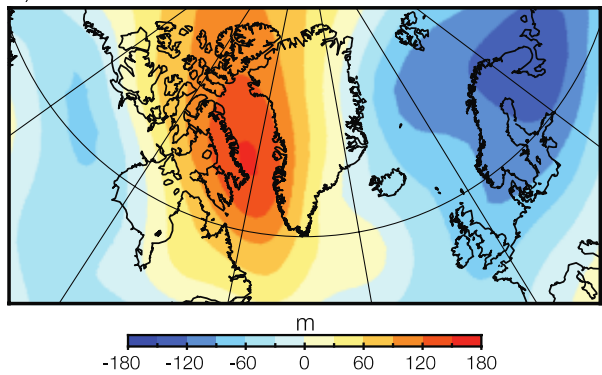
b) Sensible Heat Flux



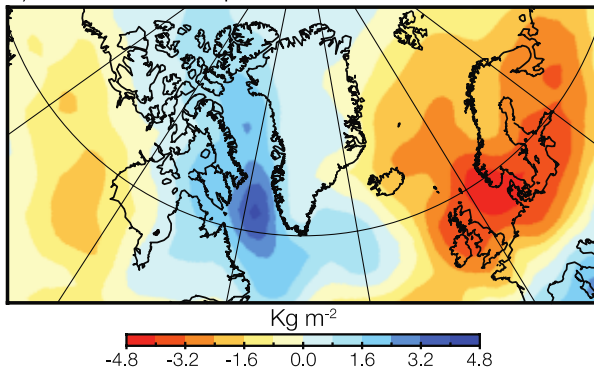
c) 500 hPa Omega



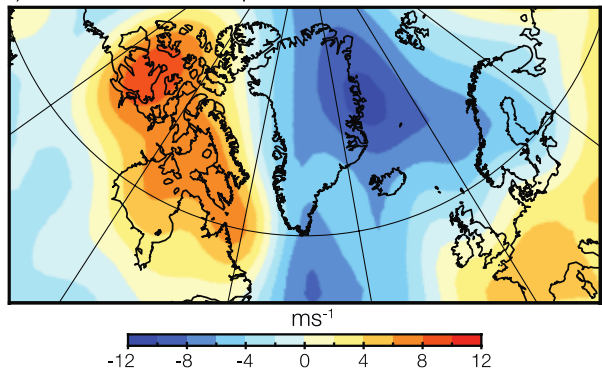
d) 1000-500hPa Thickness



e) Columnar Precipitable Water



f) Meridional wind speed



620
621
622
623
624
625
626
627
628

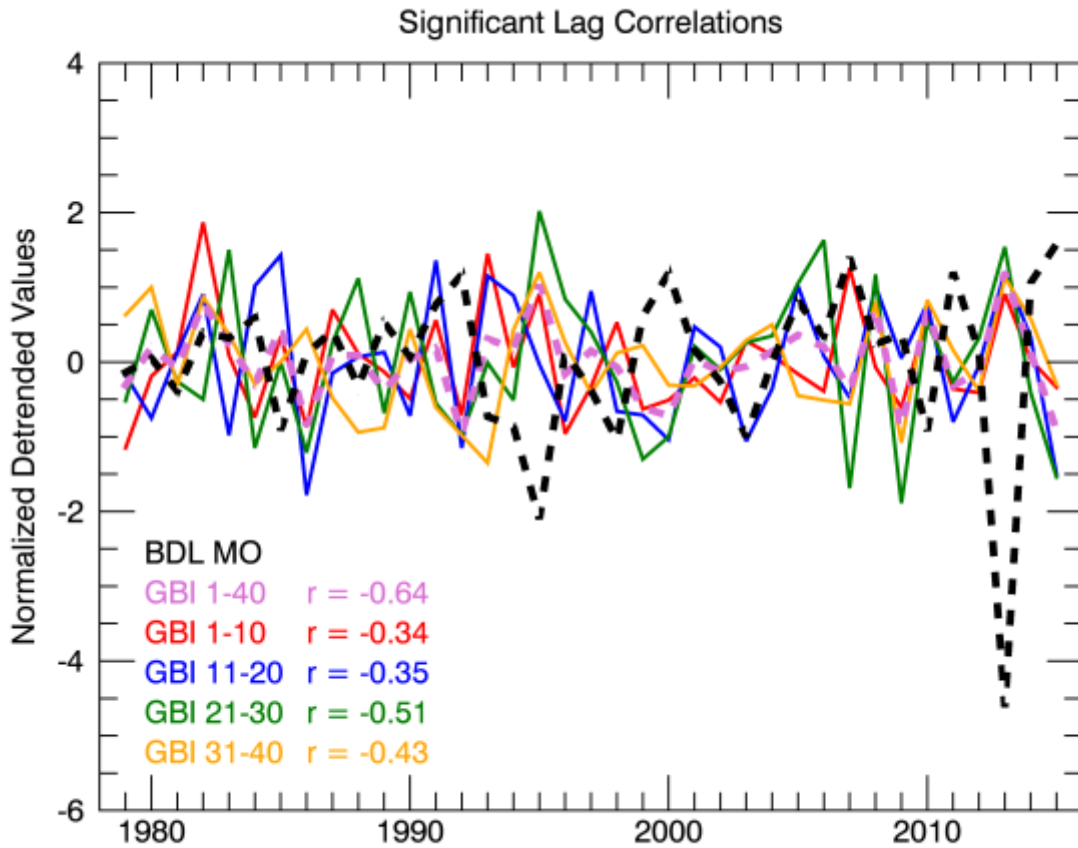
Fig. 8. Composite plots of a) latent heat flux b) sensible heat flux, c) 500 hPa omega, d) 1000-500 hPa thickness, e) columnar precipitable water, and f) meridional wind speed for the 40-days preceding 2013 BDL melt onset relative to the 1981-2010 climatology for the time period.

629 **Supplemental Table**
 630

Time Period	GBI Descriptive Statistics		Σ GBI days (n)					
	μ	σ	≤ -2	≤ -1	≤ 0	> 0	≥ 1	≥ 2
Climatology (1981-2010)	0.10	0.29	0.13	6.03	19.73	20.27	7.67	2.23
1984	-0.31	1.09	-	14	29	11	6	2
1992	-0.89	0.57	-	14	38	2	1	-
1982	0.75	1.15	-	-	15	25	17	7
1983	0.22	1.27	-	11	16	24	13	2
1980	0.14	0.66	-	-	18	22	6	-
1991	0.24	1.28	-	7	21	19	10	5

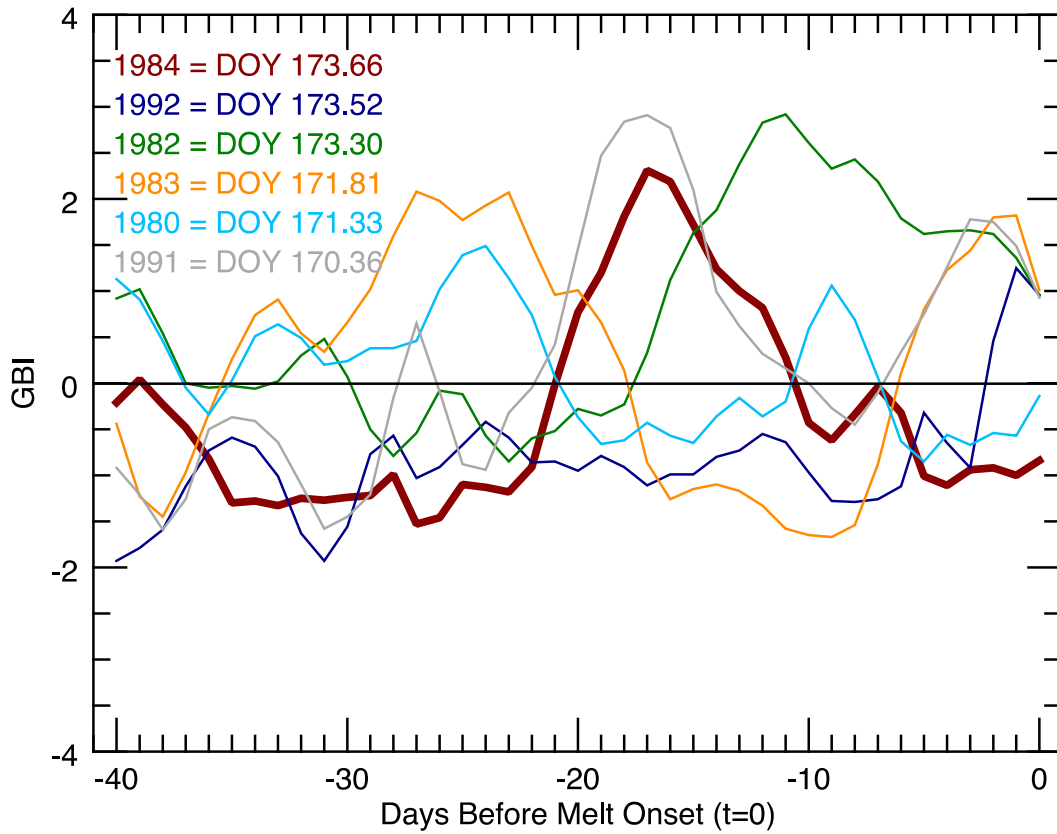
631
 632 **Supplemental Table 1.** GBI descriptive statistics (mean= μ , sigma= σ) and sum (Σ) of days
 633 at different GBI value thresholds for the 40-day period preceding MO across the
 634 climatological normal period and the late melt years (1σ above the 1981-2010 mean).
 635 Significant differences, determined by a two-tailed t-test ($p \leq 0.05$), between GBI
 636 occurrences in the six year's presented and climatology are shown in bold (where
 637 threshold of occurrence is at least 5% of days, $n=2$).
 638
 639
 640

641 **Supplemental Figures**
642

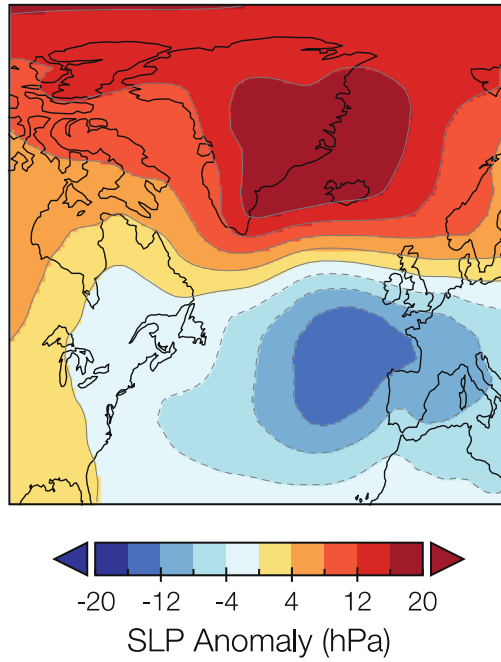


643
644
645
646
647
648
649

Supplemental Fig. 1. Time series of the significant lag correlations between normalized and detrended BDL melt onset (MO; black) and composite GBI values within daily periods preceding BDL MO (colors), 1979-2015 (following **Table 1**). All coefficients listed are significant at $p \leq 0.05$.

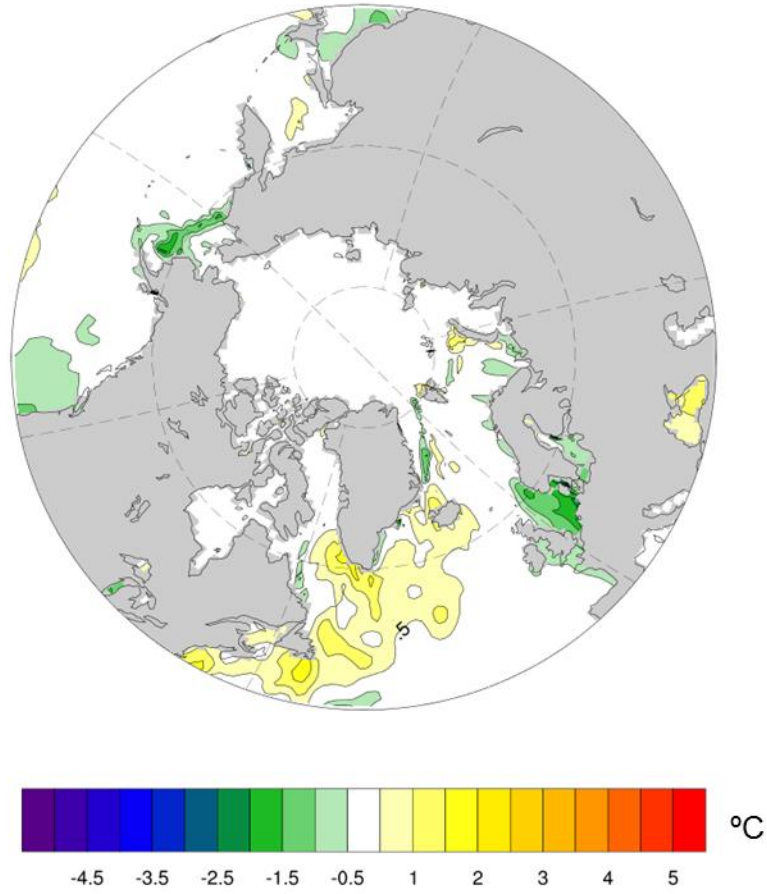


650
 651 **Supplemental Fig. 2.** Daily GBI values during the 40-days preceding the late BDL MO years
 652 (1σ above the 1981-2010 mean), which are listed sequentially in the top left of the plot
 653 with the corresponding day of year (DOY) marking continuous melt conditions for the
 654 region.
 655



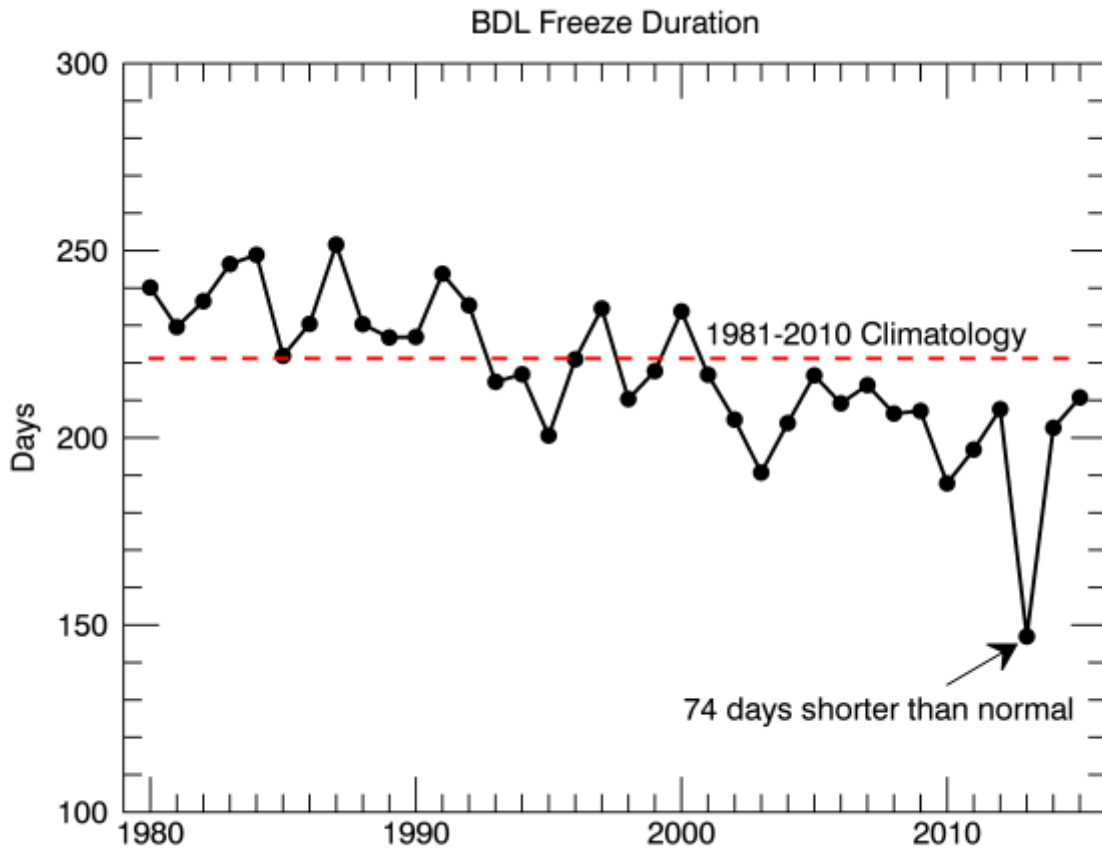
656
657
658
659
660

Supplemental Fig. 3. North Atlantic composite SLP anomaly field from 3 March – 11 April 2013 relative to 1981-2010 mean for the 40-day period.



661
662
663
664

Supplemental Fig. 4. March 2013 HadISST1 SST anomalies versus the 1981-2010 March mean.



665
 666
 667
 668
 669
 670
 671

Supplemental Fig. 5. Time series of BDL freeze duration from 1980-2015. Freeze duration reflects the time period (i.e. days) from freeze onset observed during the previous autumn season to MO occurrence the following spring.